ISSN 1990-7931, Russian Journal of Physical Chemistry B, 2017, Vol. 11, No. 8, pp. 1288–1295. © Pleiades Publishing, Ltd., 2017.
Original Russian Text © M.Yu. Tsvetkov, N.V. Minaev, A.A. Akovantseva, G.I. Pudovkina, P.S. Timashev, S.I. Tsypina, V.I. Yusupov, A.E. Muslimov, A.V. Butashin, V.M. Kanevsky, V.N. Bagratashvili, 2017, published in Sverkhkriticheskie Flyuidy. Teoriya i Praktika, 2017, Vol. 12, No. 2, pp. 68–80.

Etching of Sapphire in Supercritical Water at Ultrahigh Temperatures and Pressures under the Conditions of Pulsed Laser Thermoplasmonics

M. Yu. Tsvetkov[a, *], N. V. Minaev[a], A. A. Akovantseva[a], G. I. Pudovkina[a], P. S. Timashev[a], S. I. Tsypina[a], V. I. Yusupov[a], A. E. Muslimov[b], A. V. Butashin[b], V. M. Kanevsky[b], and V. N. Bagratashvili[a, c]

[a] *Institute of Photonic Technologies, Crystallography and Photonics Federal Scientific Research Center, Russian Academy of Sciences, Troitsk (Moscow), Russia*

[b] *Institute of Crystallography, Crystallography and Photonics Federal Scientific Research Centre, Russian Academy of Sciences, Moscow, Russia*

[c] *Department of Chemistry, Moscow State University, Moscow, 119234 Russia*

**e-mail: mtsvet52@mail.ru*

Received April 20, 2017

Abstract—The method of thermoplasmonic laser-induced backside wet etching (TPLIBWE) is applied for effective and well-controlled microstructuring of sapphire. The method is based on the generation of highly absorbing silver nanoparticles in the course of the pulsed-periodic laser irradiation. The silver nanoparticles are formed as a result of the reduction of a water-dissolved precursor, $AgNO_3$. The process of sapphire etching occurs via the formation of supercritical water at ultrahigh temperatures and pressures (which significantly exceed the critical values for water) and the formation of silver nanoparticles at the sapphire/water interface as a result of the absorption of laser radiation. The mechanism of TPLIBWE is considered and the etching rate, which reaches ~100 nm/pulse, is determined. The formation of aluminum nanoparticles, which indicates a deep destruction of Al_2O_3 as a result of TPLIBWE, is observed.

Keywords: sapphire, laser backside wet etching, microstructuring, thermoplasmonic, supercritical water, ultrahigh pressures and temperatures

DOI: 10.1134/S1990793117080127

INTRODUCTION

Synthetic sapphire (leucosapphire, Al_2O_3) is increasingly used in micro- and optoelectronics, mechanical engineering and instrument engineering, and the medical and jewelry industries. High optical uniformity and transparency in a wide range of wavelengths, small residual stresses, and radiation resistance are combined in sapphire with good mechanical, thermo-oxidative, and dielectric properties, which ensure the operation of sapphire products under high temperatures and pressures and in contact with corrosive media [1, 2].

The production of microstructures on the sapphire surface is in great demand. Microstructuring of sapphire can be used to create substrates for light-emitting structures [3]; antireflective coatings for far infrared radiation [4]; and other structures for microelectronics, photonics, and microfluidics [5]. However, the high hardness and chemical resistance of sapphire make its treatment (mechanical, ultrasonic, or chemical) a rather complicated task. Laser processing technologies of sapphire, particularly its treatment under the action of femtosecond laser pulses (see, for example, [6–8]), have been developed in recent years in addition to the traditional treatment methods.

One of the modern approaches to the laser microstructuring of sapphire (and other optically transparent materials) is the method of laser-induced backside wet etching (LIBWE) [9]. In this process, high-intensity laser radiation (usually a periodic sequence of pulses of nanosecond duration) is focused on the backside of a transparent sample, which is located in a cuvette filled with a highly absorbing liquid. Numerous processes occur in the focusing region of the sample/liquid surface (nonlinear absorption; absorption on defects; thermal, hydrodynamic, and photochemical processes; formation of a supercritical medium; formation and collapsing of bubbles; melting; evaporation; etc.). These processes can cause etching of the sample surface (i.e., the removal of its near-surface layer) [10–12]. The dominant mechanisms of LIBWE, the material removal rate, and the parameters

of the formed microstructures are determined by the type of the material, the composition of the liquid, and the parameters of the pulsed laser radiation.

As has been shown in our studies [13–16], the most important process in the LIBWE of glass is the interaction of glass with supercritical water (SCW) formed near the surface of the sample during rapid pulsed heating of the water by a laser (the critical parameters for water are $T_{cr} = 647.1$ K and $P_{cr} = 22.1$ MPa). As for sapphire, it is considered chemically resistant to SCW at temperatures below 800 K and pressures below 60 MPa (see, for example, brilliant review [17] by Yu.E. Gorbatyi and references cited therein). Sapphire windows were used in spectroscopic cuvettes with SCW and the rate of their SCW etching was negligible even at very high T and P values.

As we show in the present study, laser-induced backside wet etching makes it possible to obtain SCW at much higher temperatures and pressures than the above-mentioned values for brief periods of time (10^{-8} s) and to carry out effective etching and microstructuring of sapphire (also see [18]). This is achieved, in particular, by implementing the so-called thermoplasmonic effect [19, 20], which makes it possible to reach ultrahigh temperatures ($T \gg T_{cr}$) and pressures ($P \gg P_{cr}$) via highly absorbing plasmon nanoparticles and to carry out thermoplasmonic laser-induced backside wet etching (TPLIBWE) at a sufficiently high rate, thereby obtaining well-controlled microstructures on the sapphire surface.

EXPERIMENTAL

The basic outline of the experiment and the experimental setup were similar to those presented in our papers [13, 14] devoted to the LIBWE of glass. Sapphire (0001) substrates with a diameter of 50.8 mm and a thickness of 0.45 mm were used as optical samples. The substrates were obtained from sapphire monocrystals grown by the Kyropoulos–Musatov method [21]. Preforms of the substrates were cut with diamond saws and bits; abrasive powders or diamond and boron-carbide-based instruments were used for their polishing. Two-sided chemical–mechanical polishing of the layers was carried out with a silicasole-based suspension on a polyurethane lapping tool. All operations were completed by washing the preforms and measuring the controlled parameters. In particular, the relief and roughness of the surface after the mechanical treatment were measured using a mechanical profilometer. After the chemical–mechanical polishing, these parameters were measured by atomic-force microscopy and X-ray scattering.

We used a TECH-527 Basic diode-pumped solid-state laser (Laser-compact, Russia) at the wavelength of $\lambda = 527$ nm, the pulse duration of $\tau = 5$ ns, the maximum pulse energy of $E = 250$ μJ, and the beam divergence of <3 mrad. An etchable plate was positioned as a front wall in a demountable cell, which was then filled with the working liquid: a saturated 5 M aqueous solution of silver nitrate, $AgNO_3$ (the laser-induced decomposition of which ensured generation of highly absorbing silver nanoparticles in the system and the thermoplasmonic effect). The cell that contained the sample and the working liquid was placed on an 8MT167-100 three-axis translation stage (Standa) with the positioning accuracy of no worse than 0.2 μm. A 10x LMH-10X-532 objective (Thorlabs) with a numerical aperture of NA = 0.25 was used to focus light on the backside of the plate. Visual express monitoring of the craters and channels formed during the TPLIBWE experiments was carried out using an image obtained from a video camera. Using a dichroic mirror, a laser beam of a Gaussian profile with given energy and geometric parameters (see below) was directed on the objective and focused at the interface between the liquid and the backside of the transparent sapphire sample. The use of the selective mirror made it possible to record an image of the etched surface region via an EXCCD USB 2.0 camera (ToupTek) while illuminating the region with white light from an illuminator. This provided an accurate adjustment of the sample and the possibility to observe the treated surface during the etching.

The geometry, shape, and surface characteristics of the microstructures generated in the samples were studied using optical microscopy, scanning electron microscopy (SEM), and atomic-force microscopy (AFM). Optical images of the laser structures were obtained at different energy densities of laser pulses using an HRM-300 optical microscope (Huvitz, Korea), which supports three-dimensional visualization of the surface topography, and a Contour GT-K optical profilometer (Bruker). SEM images were obtained on a Phenom ProX scanning electron microscope at an accelerating voltage of 10 kV. AFM images were obtained on a scanning probe of the Integra-TERMA nano-laboratory (NT-MDT, Russia) that was equipped with RTESP silicon cantilevers (Veeco) with a resonant frequency of 300–360 kHz and a cantilever tip radius of less than 5 nm. The scanning was carried out in a semicontact mode in air at a constant amplitude (topography). The electron absorption spectra of the working liquid were recorded on a Cary 50 spectrometer (Varian).

Experiments on laser-plasmon microstructuring of sapphire samples were carried out at a pulse repetition rate of 1 kHz and laser radiation energies of up to 25 μJ in a pulse. The sample was irradiated both with focused (backside of the plate at the beam waist region) and defocused beams (the beam waist region was shifted into the absorbing liquid by up to 20 μm). The focusing parameters of a laser beam with a Gaussian profile are determined by the diameter of the beam in front of the focusing lens and by the parameters of the focusing optics [22]. In our case, the diameter of the beam varied from 1.4 to 4.0 mm. This made it possible to carry

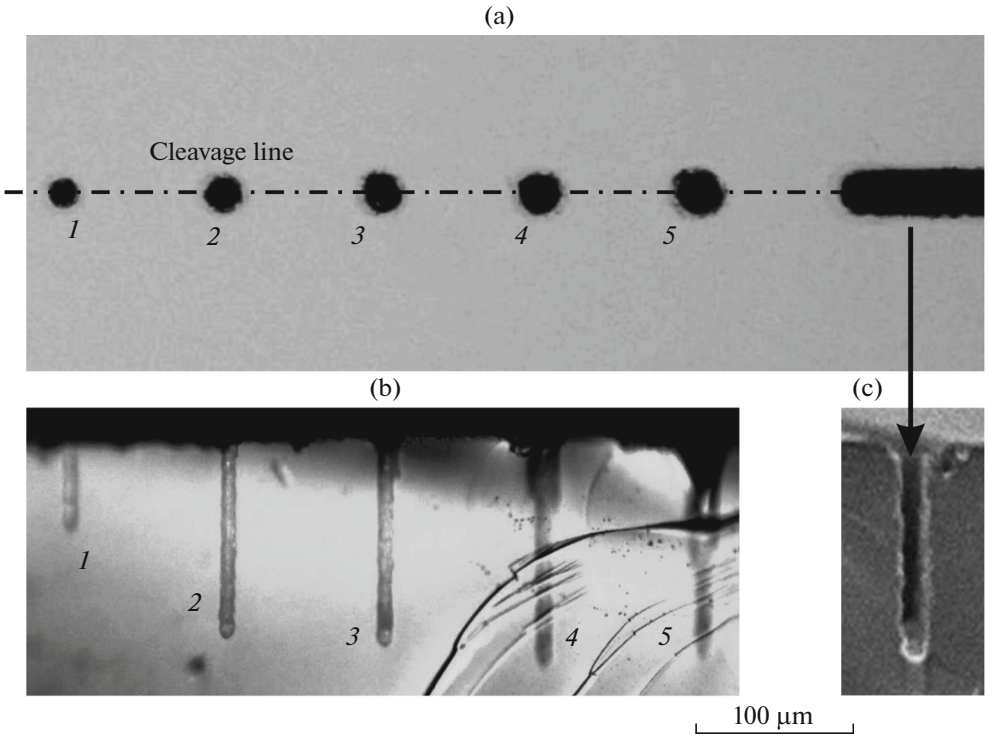

Fig. 1. Sapphire plate: a—top view; b—view of a transverse cleavage with craters (optical microscopy); c—view of a transverse cleavage with a channel (scanning electron microscopy).

out a formation near the focus region at the sample–absorbing liquid interface using the following parameters: the beam waist diameter of 3.4–9.6 μm (1/*e* level) and the focusing depth of 30–300 μm. During defocusing, the beam diameter in the etching region increased to 20 μm. The energy density reached $\Phi \approx 300$ J/cm^2 under our conditions.

Experiments on the formation of craters were carried out by varying the energy density of laser radiation Φ and the number of laser radiation pulses N and by shifting the laser beam waist relative to the backside of the plate. The channels were formed at a laser beam scan speed of 8–140 μm/s.

RESULTS

Sapphire Microstructuring

Several types of structures were formed as a result of implementing the TPLIBWE process on sapphire:

—craters were formed both in the focusing region and in the region that was irradiated by a defocused beam;

—channels were produced by scanning with a focused and a defocused beam;

—microstructures were produced by scanning the sapphire plate surface with a beam.

By smoothly changing the energy density of the laser radiation, we determined the threshold of the TPLIBWE of sapphire based on the emergence of laser craters on the sapphire surface. In our case, the threshold was $\Phi_{tr} \sim 6$ J/cm^2. When the threshold is exceeded, the etching intensity starts to increase rapidly: it reaches a value of 100 nm/pulse and higher at $\Phi \sim 30$ J/cm^2. This makes it possible to form neat craters and channels of 200 μm in depth at a rather high aspect ratio of ≥10 (Fig. 1).

The figure shows the optical and scanning electron microscopy images of the craters. The etching was carried out at a frequency of 1 kHz and an irradiation energy of $E = 12$ μJ. The number of pulses varied for craters *1*–*5*: *1*—500; *2*—2500; *3*—10000; *4*—60000; and *5*—100000. The formed craters were of 9 μm in diameter. The depth of the first crater was 60 μm and the depth of the others was 120 μm.

The transverse cleavage of the plate results from splitting of the plate along the line (see dot/dashed line in Fig. 1a) formed by the craters and channels as shown in the figure. The heterogeneity of the sapphire plate cleavage is clearly visible in the lower right-hand corner of Fig. 1b.

Figure 1a also shows that the diameter of the craters increases with increasing number of laser pulses; the crater depth increases at first but then quickly reaches saturation (at $N \geq 6000$). Moreover, the crater quality clearly deteriorates at sufficiently large N (Fig. 1b, channels *4* and *5*). In particular, the channel entry significantly widens, which can be naturally associated

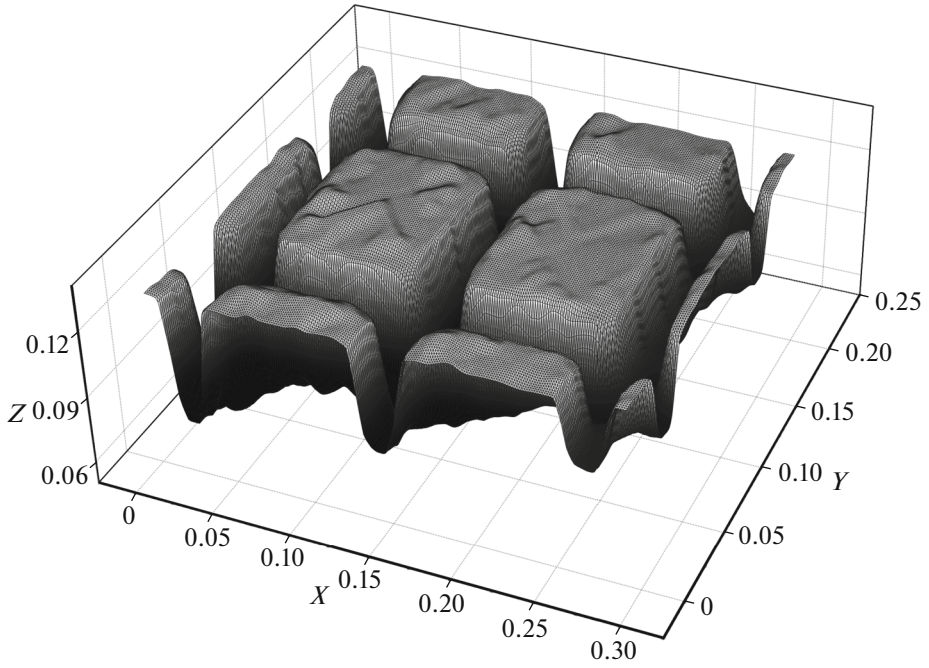

Fig. 2. Fragment of a microstructure. The 3D image was obtained on a 3D optical microscope.

with an increasingly strong impact on the material at the wings of the Gaussian distribution F at increasing N.

The sapphire etching intensity continues to increase with increasing value of Φ. However, the quality of the channels significantly deteriorates at sufficiently large Φ (>100–150 J/cm^2). At Φ > 300 J/cm^2, the removal of the material is no longer manifested as relatively smooth craters, but takes the form of poorly controlled and irregular pits, while the ejection products rise above the sapphire surface. We associate this with the dominance of hydrodynamic cavitation processes, which cause the intensive removal of superheated (softened) sapphire. Despite its high etching intensity (microns per pulse), this "intense mode" of TPLIBWE is unsuitable for regular and well-controlled etching of sapphire.

The developed TPLIBWE technology made it possible to form microstructures of different types. As an example, Fig. 2 shows a microstructure that we formed to create prototypes of structured biosubstrates.

The distance between the channels is 100 μm, the channel width (at the top) is 35 μm, and the depth is 55 μm.

Formation of Nanoparticles

Two types of processes that lead to the formation of nanoparticles occur upon the action of laser radiation on the sapphire surface in a solution of silver nitrate. The first process, which predominates at the initial stage of etching, is associated with the reduction of $AgNO_3$, the formation of silver nanoparticles (nanoAg), and the formation of the plasmon medium [23]. The second process is a deep decomposition of sapphire as a result of its exposure to SCW and the subsequent formation of aluminum nanoparticles (nanoAl) [24–26]. As a result, both types of particles (nanoAg and nanoAl) can be found in the working liquid at the end of the etching process. Their plasmonic peaks are clearly traced in the extinction spectrum of the working liquid after the completion of the TPLIBWE process (Fig. 3a).

The peak at 460 nm and the absence of additional peaks in the longwave region indicate the emergence of spherical nanoAg with average diameters of slightly more than 50 nm in the working liquid [27]. The peak at 300 nm is typical of aluminum nanoparticles with diameters of up to several tens of nanometers [25, 28]. Figure 3b shows an AFM image of Al nanoparticles deposited on a silicon substrate. Separation of nanoAg and nanoAl was performed by decanting until the plasmon resonance of silver disappeared. Subsequently, the exclusive deposition of nanoAl on the substrate was confirmed by energy dispersive X-ray analysis (EDAX).

The forming nanoparticles are in the spent solution. Moreover, a considerable amount of them is deposited on the surface of the sapphire plate that is being processed and in the pores of the microstructures that are formed. We used nitric acid mixed with water in a ratio of 1 : 3 to etch the nanoparticles. To ensure access of the etchant to the pores with a large

aspect ratio, we used treatment in an ultrasonic bath. The samples were then washed with deionized water.

DISCUSSION

Thus, the performed experiments demonstrated the possibility of an efficient formation of well-controlled microstructures on the sapphire surface under conditions of thermoplasmonic laser-induced backside wet etching.

Formation of a Plasmon Medium

In our TPLIBWE experiments, silver nanoparticles are formed upon the reduction of $AgNO_3$ by laser irradiation of its aqueous solution. Laser radiation initiates the formation of silver Ag^0 atoms in the solution [23, 29]. Then, the process of self-assembly takes place and it is accompanied by the formation of nanoAg of various sizes [30, 31].

It is important to note that, when a fresh solution of $AgNO_3$ is used, the start of laser irradiation is always followed by an incubation period during which the etching is negligible but the formation of silver nanoparticles is intense. After that, the etching process begins.

It is known that silver nanoparticles smaller than 40–50 nm in size are characterized by resonant plasmon absorption at 400 nm and that the peak of plasmon absorption shifts to the longwave region as the nanoparticles grow [27].

When analyzing the absorption spectra of an aqueous colloid obtained after the TPLIBWE of a sapphire sample, we directly observed the formation of nanoAg. The rather broad absorption peak near 460 nm is precisely due to nanoAg of different sizes formed in the working liquid. This peak was missing in the initial (unirradiated) working liquid.

As for the question of the mechanism of the formation and growth of nanoAg during the incubation period, we will not go into this in detail. However, we note that, besides laser photolysis (and photothermolysis) of silver nitrate (including that adsorbed on the sapphire surface), traces of nanoAg in the working liquid can also have a role.

The first "seeding" pulses of laser radiation form centers of additional plasmon absorption and the process develops incrementally (among other things, via thermal decomposition of $AgNO_3$ near the silver nanoparticles that are heated by pulsed laser radiation). As a result, a region with a high density of strongly absorbing nanoAg is formed at the interface with the treated sample. Laser pulses turn such nanoparticles into highly localized heat sources with huge energy release at the sample/liquid interface; as a result, both thermal and hydrodynamic processes are initiated and these processes lead to the removal of some of the sample material (etching) [32, 33].

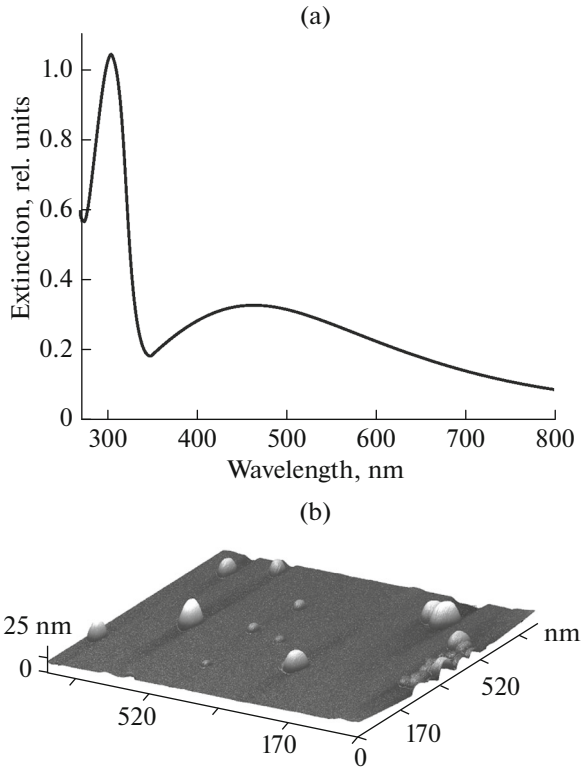

Fig. 3. (a) Extinction spectrum of the nanoparticle suspension obtained after the TPLIBWE processing of sapphire: the peak at 300 nm is due to nanoAl and the peak at 460 nm is due to nanoAg; (b) 3D AFM image of nanoAl that were deposited from the working liquid on a silicon substrate after TPLIBWE.

A detailed description of the mechanisms and dynamics of sapphire TPLIBWE is extremely complex because there are numerous processes (chemical, thermal, hydrodynamic, etc.) that depend on the parameters of laser radiation and the properties of the material. For example, it is necessary to account for possible reactions of thermolysis of Al_2O_3 [34].

It is clear, however, that the very possibility of efficient etching and microstructuring of sapphire is associated with achieving ultrahigh temperatures and pressures at the sapphire/water interface in the supercritical region.

Estimates of Temperatures and Pressures

Let us note once again that etching of sapphire via the TPLIBWE process with an aqueous solution of $AgNO_3$ occurs because of the absorption of laser pulses by silver nanoparticles that are actively formed at the sapphire/liquid interface. The absorption of a short laser pulse by Ag nanoparticles causes their rapid heating, which, in turn, facilitates equally rapid heating of a thin layer of sapphire and liquid near the interface. All this causes a rather rapid etching of sapphire.

It is obvious that the maximum intensity of etching of the sample surface will occur at the maximum temperatures, which are reached by the end of a laser pulse. In this case, the absorbed energy density Φ of a laser impulse is used to heat three layers: the layer of silver with a thickness of d and the layers of sapphire and water that are adjacent to the silver layer. The thicknesses of the latter layers are determined by the corresponding thermal heating depths $d_T = \sqrt{4D_T\tau}$, where D_T is the thermal diffusivity coefficient and τ is the duration of the laser pulse. By the end of the laser pulse, these three layers will be heated to a temperature of

$$T = T_0 + \frac{\Phi_{abs}}{\rho^A C_p^A d + \rho^S C_p^S d_T^S + \rho^L C_p^L d_T^L},$$

where $T_0 \approx 300$ K is the initial temperature; Φ_{abs} is the part of Φ that is absorbed in the layer of silver; ρ is the density; C_p is the specific heat capacity; and the upper indices A, S, and L refer to silver, sapphire, and liquid, respectively.

To estimate Φ_{abs}, we will assume that a monolayer of silver nanoparticles covers half of the sapphire surface in the region of the laser action over the interval between successive laser pulses. Given that the coefficient of effective absorption of nanoAg at the wavelength of the laser radiation (527 nm) is 0.3 [34], we get $\Phi_{abs} \approx 0.15\Phi$. In this case, we get $\Phi_{abs} \approx 0.9$ J/cm^2 for the threshold values of $\Phi \sim 6$ J/cm^2. By applying the reference values $C^A = 10\,500$ kg/m^3, $C^L = 1000$ kg/m^3, $C^S = 3\,980$ kg/m^3, $C_p^A = 240$ J/(kg K), $C_p^L = 4200$ J/(kg K), $C_p^S = 850$ J/(kg K), $D_T^L = 1.4 \times 10^{-7}$ m^2/s, $D_T^S = 4 \times 10^{-6}$ m^2/s, and $\tau = 5 \times 10^{-9}$ s in (3), we get $T \approx 7 \times 10^3$ K for $\Phi_{abs} = 0.9$ J/cm^2 and $d = 10$ nm. Thus, our estimates show that the absorption of a laser pulse can heat thin layers of sapphire ($D_T^S \approx 280$ nm) and liquid ($d_T^L \approx 50$ nm) to ultrahigh temperatures $T \gg T_{cr}$.

The possibility of achieving ultrahigh temperatures of water $T \gg T_{cr}$ during TPLIBWE of sapphire under our conditions is also indirectly confirmed by the fact of the formation of nanoAl, which is directly observed in the working liquid by the electron absorption spectra (Fig. 3a) and by the AFM images after deposition on the surface (Fig. 3b). The emergence of nanoAl is caused by self-assembly of Al atoms, which, according to [34] can be formed as a result of the thermolysis of aluminum oxide at ultrahigh pressures and temperatures.

For a series of N laser pulses with the duration of τ, the total action time of an ultrahigh temperature on sapphire can be estimated as $\tau_N \approx N\tau$. Under our experimental conditions ($\tau = 5 \times 10^{-9}$ s and $N < 10^5$ pulses), the total action time is $\tau_N < 5 \times 10^{-4}$ s. It follows from our experiments that, under these conditions, sapphire is efficiently etched to the depth of 100–200 μm. However, as already noted in the introduction, sapphire is chemically resistant to SCW at temperatures below ~800 K and pressures below ~60 MPa; i.e., its etching over "macroscopic" times of ~10^4–10^5 (hours, days) is negligible [17]. Unfortunately, we are not yet able to experimentally determine the temperature that is achieved at the sapphire/water interface under the conditions of TPLIBWE. It is clear, however, that the temperature of the liquid and the surface can rise to ultrahigh values (up to several thousand K).

As for the impulse pressures P that are reached in the process of TPLIBWE, our measurements performed using an acoustic needle hydrophone [16] revealed pressure impulses of $P \geq 500$ MPa, which significantly exceed the critical pressure for water (22.1 MPa).

In our opinion, pressures and temperatures as high as those achieved in the TPLIBWE process provide the possibility of implementing a sufficiently high intensity of sapphire etching (up to 100 nm/pulse and higher), which is recorded experimentally.

Figure 4 shows a diagram that explains the mechanism proposed by us for the process of thermoplastic etching of sapphire performed in a multipulse mode at different time periods after the start of irradiation by a sequence of laser pulses.

The action of the first laser pulses on the $AgNO_3$ solution (Fig. 4a) leads to the formation of silver atoms, which merge into nanoAg (*2*) in the bulk liquid and at the sapphire/water interface, forming, as we assume, an island film (*6*) on the surface. After several dozen pulses (b), the laser radiation energy begins to be absorbed in the strongly localized region that is formed on the sapphire surface and near it by an increasing concentration of nanoAg. The absorption of laser energy leads to the rapid heating ($T \gg T_{cr}$) of the nanoparticles (thermoplasmonics) and the adjacent layers of sapphire and water and to the rapid growth of the pressure ($P \gg P_{cr}$). Impulse etching of the softened sapphire surface with supercritical water occurs at this stage, which leads to the formation of Al atoms and, subsequently, nanoAl (*3*). Hydrodynamic flows (*4*) arise in the vicinity of the laser action region: these flows carry some of the nanoAg and nanoAl deep into the solution. The action of a large number of pulses (c) on the laser action zone leads to the formation of a crater. After every new pulse, the bottom and walls of this crater get covered with etching products, particularly, with nanoAg (*6*). Consequently, sapphire gets etched rather efficiently to the depth of 200 μm and deeper despite the relatively small total time of the multipulse action ($\tau_N < 5 \times 10^{-2}$ s). This is due to the ultrahigh temperatures and pressures that are reached during TPLIBWE.

Note that the intense hydrodynamic flows that are formed during the TPLIBWE process can have a significant effect on the mechanism and etching rate. In addition to heating, it is necessary to consider different

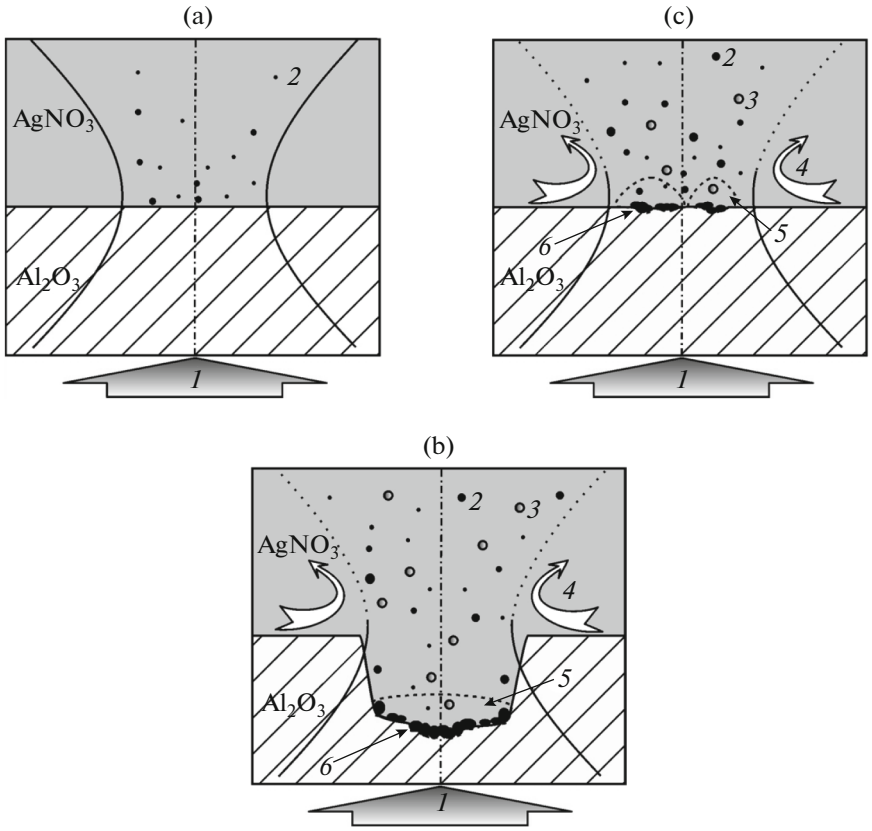

Fig. 4. Action mechanism of the thermoplasmic etching of sapphire in a multipulse mode at the following time periods: (a) after the first pulses; (b) after a small series of pulses (the beginning of etching); and (c) after a large series of pulses (deep etching): *1*—laser beam; *2*—nanoAg; *3*—nanoAl; *4*—hydrodynamic flows; *5*—formation of supercritical water (SCW); and *6*—silver nanoparticles localized near the sapphire surface.

cooling processes that are caused by the generation of the hydrodynamic flows. Such flows can ensure the removal of etch products and the delivery of a "fresh" working medium to the etching area of the material. All in all, the transport processes stimulated by TPLIBWE require separate consideration.

CONCLUSIONS

The method of thermoplasmonic laser-induced backside wet etching (using a pulsed-periodic laser with a wavelength of 527 nm and a pulse duration of 5 ns) has been used for efficient and well-controlled microstructuring of sapphire. The method is based on the generation of highly absorbing plasmon silver nanoparticles as a result of the laser destruction of water-dissolved $AgNO_3$. Sapphire is etched by supercritical water that is formed at the sapphire/water interface as a result of the absorption of laser radiation by silver nanoparticles at ultrahigh temperatures and pressures. The mechanism of TPLIBWE has been proposed and the etching intensity, which reaches 100 nm/pulse and higher, has been determined. The formation of aluminum nanoparticles, which indicates a deep destruction of Al_2O_3 in the TPLIBWE process, has been observed.

ACKNOWLEDGMENTS

This work was supported by the Russian Science Foundation, project no. 14-33-00017-P (development of the technology of thermoplasmonic laser-induced backside wet etching and study of the processes of sapphire etching with supercritical water at ultrahigh temperatures and pressures) and by the Russian Foundation for Basic Research, project OFI-M no. 16-29-11763 (preparation of sapphire plate samples and diagnostics of the formed structures).

We thank Professor M.G. Kiselev for helpful discussions of the results.

REFERENCES

1. E. R. Dobrovinskaya, L. A. Lytvynov, and V. V. Pishchik, *Sapphire. Material Manufacturing, Applications*. (Springer, New York, 2009).
2. *Sapphire: Structure, Technology, and Application*, Ed. by I. Tartaglia (Nova Science, New York, 2013).

3. L. Kuna, A. Haase, F. Reil, C. Sommer, J. R. Krenn, P. Hartmann, P. Pachler, S. Tasch, and F. P. Wenzl, IEEE J. Sel. Top. Quantum Electron. **15**, 1250 (2009).
4. T. Matsumura, K. Young, Q. Wen, S. Hanany, H. Ishino, Y. Inoue, M. Hazumi, J. Koch, O. Suttman, and V. Schütz, Appl. Opt. **55**, 3502 (2016).
5. T. B. Teplova and A. S. Samerkhanova, Gorn. Inform.-Anal. Byull., No. 10, 338 (2006).
6. M. Hörstmann-Jungemann, J. Gottman, and M. Keggenhoff, J. Laser Micro/Nanoeng. **5**, 145 (2010).
7. Q. Li, Y. Yu, L. Wang, X. Cao, X. Liu, Y. Sun, Q. Chen, J. Duan, and H. Sun, IEEE Photon. Technol. Lett. **28**, 1290 (2016).
8. M. Liu, Y. Hu, X. Sun, C. Wang, J. Zhou, X. Dong, K. Yin, D. Chu, and J. Duan, Appl. Phys. A **123**, 99 (2017).
9. K. Zimmer, M. Ehrhardt, and R. Böhme, in *Laser Ablation in Liquids: Principles and Applications in the Preparation of Nanomaterials*, Ed. by G. Yang (Pan Stanford, Singapore, 2012).
10. H. Niino, Y. Yasui, X. Ding, A. Narazaki, T. Sato, Y. Kawaguchi, and A. Yabe, J. Photochem. Photobiol. A: Chem. **158**, 179 (2003).
11. C. Vass, J. Budai, Z. Schay, and B. Hopp, J. Laser Micro/Nanoeng. **5**, 43 (2010).
12. K. Zimmer, R. Böhme, M. Ehrhardt, and B. Rauschenbach, Appl. Phys. A **101**, 405 (2010).
13. M. Yu. Tsvetkov, V. I. Yusupov, N. V. Minaev, A. A. Akovantseva, P. S. Timashev, K. M. Golant, B. N. Chichkov, and V. N. Bagratashvili, Opt. Laser Technol. **88**, 17 (2017).
14. M. Yu. Tsvetkov, V. I. Yusupov, P. S. Timashev, K. M. Golant, N. V. Minaev, S. I. Tsypina, and V. N. Bagratashvili, Sverkhkrit. Fluidy Teor. Prakt. **11** (2), 14 (2016).
15. M. Yu. Tsvetkov, V. I. Yusupov, N. V. Minaev, P. S. Timashev, K. M. Golant, and V. N. Bagratashvili, Laser Phys. Lett. **13**, 106001 (2016).
16. M. Yu. Tsvetkov, V. I. Yusupov, and P. S. Timashev, K. M. Golant, N. V. Minaev, and V. N. Bagratashvili, Nanotechnol. Russ. **12**, 86 (2017).
17. Yu. E. Gorbatyi, Sverkhkrit. Fluidy Teor. Prakt. **2** (1), 40 (2007) [in Russian].
18. S. I. Dolgaev, A. A. Lyalin, A. V. Simakin, and G. A. Shafeev, Quantum Electron. **26**, 65 (1996).
19. A. O. Govorov and H. H. Richardson, Nanotoday **2**, 30 (2007).
20. G. Baffou and R. Quidant, Laser Photon. Rev. **7**, 171 (2013).
21. V. E. Asadchikov, A. V. Butashin, V. M. Kanevsky, A. E. Muslimov, and B. S. Roshchin, in *Sapphire: Structure, Technology, and Application*, Ed. by I. Tartaglia (Nova Science, New York, 2013), p. 35.
22. A. E. Siegman, *Lasers* (Univ. Science Books, Mill Valley, CA, 1986).
23. M. Sakamoto, M. Fujistuka, and T. Majima, J. Photochem. Photobiol. C: Photochem. Rev. **10**, 33 (2009).
24. H. Varel, M. Wahmer, A. Rosenfeld, D. Ashkenasi, and E. E. B. Campbell, Appl. Surf. Sci. **127–129**, 128 (1998).
25. G. L. Homyak, K. L. N. Pbani, D. L. Kunkel, V. P. Menon, and C. R. Martin, Nanostruct. Mater. **6**, 839 (1995).
26. E. K. Kazenas and Yu. V. Tsvetkov, *Oxide Evaporation* (Nauka, Moscow, 1997) [in Russian].
27. N. G. Khlebtsov and L. A. Dykman, J. Quant. Spectrosc. Rad. Transfer **111**, 1 (2010).
28. E. Stratakis, M. Barberoglou, C. Fotakis, G. Viau, C. Garcia, and G. A. Shafeev, Opt. Express **17**, 12650 (2009).
29. A. Yu. Olenin and G. V. Lisichkin, Russ. Chem. Rev. **80**, 605 (2011).
30. U. Kreibig, M. Gartz, A. Hilger, H. Hövel, M. Quinten, D. Wagner, and H. Ditlbacher, in *Functional Properties of Nanostructured Materials*, Ed. by R. Kassing et al. (Springer, 2005).
31. M. Yu. Tsvetkov, V. N. Bagratashvili, V. Ya. Panchenko, A. O. Rybaltovskii, M. I. Samoilovich, and M. A. Timofeev, Nanotechnol. Russ. **6**, 619 (2011).
32. Z. Yan and D. B. Chrisey, J. Photochem. Photobiol. C: Photochem. Rev. **13**, 204 (2012).
33. V. Amendola and M. Meneghetti, Phys. Chem. Chem. Phys. **15**, 3027 (2013).
34. L. Zhdan, V. Kovalenko, N. Strelenko, and Y. Chvertko, Soldag. Insp. Sao Paulo **18**, 314 (2013).
35. E. D. Palik, *Handbook of Optical Constants of Solids II* (Academic, New York, 1998).

Translated by Yu. Modestova